

The unluckiest star: A spectroscopically confirmed repeated partial tidal disruption event AT 2022dbl

ZHEYU LIN ^{1,2} NING JIANG ^{1,2} TINGGUI WANG ^{1,2,3} XU KONG ^{1,2,3} DONGYUE LI ⁴ HAN HE ⁵ YIBO WANG ^{1,2}
JIAZHENG ZHU ^{1,2} WENTAO LI ^{1,2} JI-AN JIANG ^{1,2,6} AVINASH SINGH ⁷ RISHABH SINGH TEJA ^{8,9} D. K. SAHU ⁸
CHICHUAN JIN ⁴ KEIICHI MAEDA ¹⁰ AND SHIFENG HUANG ^{1,2}

¹*Department of Astronomy, University of Science and Technology, Hefei, 230026, China; linzheyu@mail.ustc.edu.cn, jnac@ustc.edu.cn, twang@ustc.edu.cn, xkong@ustc.edu.cn*

²*School of Astronomy and Space Sciences, University of Science and Technology of China, Hefei, 230026, China*

³*Institute of Deep Space Sciences, Deep Space Exploration Laboratory, Hefei 230026, China*

⁴*National Astronomical Observatories, Chinese Academy of Sciences, Beijing, 100101, China*

⁵*Department of Astronomy, School of Physics and Technology, Wuhan University, Wuhan 430072, China*

⁶*National Astronomical Observatory of Japan, 2-21-1 Osawa, Mitaka, Tokyo 181-8588, Japan*

⁷*Hiroshima Astrophysical Science Center, Hiroshima University, Higashi-Hiroshima, Hiroshima 739-8526, Japan*

⁸*Indian Institute of Astrophysics, II Block, Koramangala, Bengaluru-560034, Karnataka, India*

⁹*Pondicherry University, R.V. Nagar, Kalapet, Pondicherry-605014, UT of Puducherry, India*

¹⁰*Department of Astronomy, Kyoto University, Kitashirakawa-Oiwake-cho, Sakyo-ku, Kyoto 606-8502, Japan*

ABSTRACT

The unluckiest star orbits a supermassive black hole elliptically. Every time it reaches the pericenter, it shallowly enters the tidal radius and gets partially tidal disrupted, producing a series of flares. Confirmation of a repeated partial tidal disruption event (pTDE) requires not only evidence to rule out other types of transients, but also proof that only one star is involved, as TDEs from multiple stars can also produce similar flares. In this letter, we report the discovery of a repeated pTDE, AT 2022dbl. In a quiescent galaxy at $z = 0.0284$, two separate optical/UV flares have been observed in 2022 and 2024, with no bright X-ray, radio or mid-infrared counterparts. Compared to the first flare, the second flare has a similar blackbody temperature of $\sim 26,000$ K, slightly lower peak luminosity, and slower rise and fall phases. Compared to the ZTF TDEs, their blackbody parameters, bolometric energies and light curve shapes are all similar. The spectra taken during the second flare show a steeper continuum than the late-time spectra of the previous flare, consistent with a newly risen flare. More importantly, the possibility of two independent TDEs can be largely ruled out because the optical spectra taken around the peak of the two flares exhibit highly similar broad Balmer, N III and possible He II emission lines, especially the extreme ~ 4100 Å emission lines. This represents the first robust spectroscopic evidence for a repeated pTDE, which can soon be verified by observing the third flare, given its short orbital period.

1. INTRODUCTION

An unlucky star passes too close to a supermassive black hole (SMBH). It gets tidally torn apart and produces a luminous flare. In this case, a tidal disruption event (TDE) occurs (Hills 1975; Rees 1988). Thanks to wide-field optical surveys in the past decade, such as the All-Sky Automated Survey for Supernovae (ASAS-SN; Shappee et al. 2014), the Asteroid Terrestrial-impact Last Alert System (ATLAS; Tonry et al. 2018; Smith et al. 2020) survey and the Zwicky Transient Facility (ZTF; Bellm et al. 2019), ~ 100 TDEs have been discovered (e.g., van Velzen et al. 2021; Gezari 2021; Hammerstein et al. 2023; Yao et al. 2023), despite its relatively low occurrence rate of about $10^{-4} - 10^{-5}$ galaxy⁻¹ yr⁻¹ (e.g., Wang & Merritt 2004; Stone & Metzger 2016; van Velzen et al. 2020; Yao et al. 2023). However, most of these TDEs are bright in optical/UV wavelengths but faint in X-

ray, contrary to the early prediction that most energy should be released in the UV/X-ray bands. The origin of optical/UV emission is still under debate (e.g., Piran et al. 2015; Metzger & Stone 2016; Dai et al. 2018; Lu & Bonnerot 2020; Liu et al. 2021; Thomsen et al. 2022; Guo et al. 2023), awaiting definitive observational evidence. As a result, the identification of optical/UV TDEs is empirical, relying on the features of the former samples.

A luckier star has a shallower encounter with an SMBH. Only part of it gets tidally disrupted and produces a similar flare. This is called a partial tidal disruption event (pTDE) happens. The shallowness of the encounter is usually defined by the ratio of the tidal radius and the pericenter, or the penetration factor, $\beta \equiv R_t/R_p$. Numerical simulations have found that the critical β values for the onset of the pTDE and the full TDE depend on the density profile of the star (e.g., Guillochon & Ramirez-Ruiz 2013; Law-Smith et al. 2017). The

event rate for pTDEs is predicted to be even higher than that of full TDEs (e.g., Stone & Metzger 2016; Stone et al. 2020; Chen & Shen 2021; Zhong et al. 2022), providing a boost to the total TDE rate. However, distinguishing pTDEs from full TDEs is difficult, as the luminosity is not only determined by β or the disrupted mass, but also depends on other parameters such as the radiation efficiency, the BH mass and stellar properties.

Sometimes, this stroke of luck instead leads to tragedy. The unluckiest star initially has an elliptical orbit. Each time it approaches the pericenter, it experiences partial disruption, producing a series of flares. In this special case, a repeated pTDE occurs. The mechanism that creates the unluckiest star is possibly the Hills breakup, in which a stellar binary passes by an SMBH and gets broken into a hypervelocity star and a tightly bound star (Hills 1988; Cufari et al. 2022; Lu & Quataert 2023). Repeated pTDEs can provide precious evidence for the existence of pTDEs. However, the confirmation of repeated pTDEs can be complicated by other possible scenarios, such as a double TDE caused by an extremely close encounter between a stellar binary and either an SMBH (Mandel & Levin 2015) or an mpc-scale SMBH binary (Wu & Yuan 2018). Alternatively, multiple independent TDEs could be supported by an enhanced TDE rate, due to the concentrated nuclear stellar profile, e.g., in post-starburst galaxies (e.g., Arcavi et al. 2014; Hammerstein et al. 2021; Bortolas 2022; Wang et al. 2024) or galaxies with nuclear star clusters (Pfister et al. 2020). Despite the challenges, several candidates for repeated pTDE have been reported, e.g., ASASSN-14ko (Payne et al. 2021, 2022, 2023; Huang et al. 2023), eRASSt J045650.3–203750 (Liu et al. 2023, 2024), AT2018fyk (Wevers et al. 2023), RX J133157.6–324319.7 (Hampel et al. 2022; Malyali et al. 2023) and AT2020vdk (Somalwar et al. 2023b). The great diversity of the flaring intervals, bands and shapes (listed in Table 2) among these sources calls for additional theoretical efforts.

In this letter, we report the discovery of a new recurring flare at the position of AT2022dbl (also known as AT2018mac, ZTF18abdajx, ASASSN-22ci). It follows the dissipation of the tidal disruption flare that rose two years ago. Photometric and spectroscopic follow-up observations have been conducted since this discovery, confirming that this flare is also the result of a TDE. Its extreme ~ 4100 Å emission line resembles the last flare, providing vital evidence for a repeated pTDE.

The paper is organized as follows. In Section 2, we present the observations and data reduction procedures. In Section 3, we analyze the host galaxy, the historical and recent photometric evolution in UV, optical and X-ray bands, as well as the optical spectra. In Section 4, we discuss the possible origins of AT2022dbl and compare it with other repeated pTDEs. A final summary is given in Section 5. All errors

marked with “ \pm ” represent the 1- σ confidence intervals. We assume a flat cosmology with $H_0 = 70$ km s $^{-1}$ Mpc $^{-1}$ and $\Omega_\Lambda = 0.7$. For the extinction correction, we use the extinction law of Fitzpatrick (1999), the standard extinction curve with $R_V = A_V/E(B-V) = 3.1$ (Osterbrock & Ferland 2006) and adopt a Galactic extinction of $E(B-V) = 0.0159$ mag (Planck Collaboration et al. 2016). All magnitudes are in the AB system (Oke 1974).

2. OBSERVATION & DATA REDUCTION

Since the discovery of the recurring flare on January 22, 2024, we have performed extensive photometric and spectroscopic observations. Meanwhile, we have also collected historical photometric and spectroscopic data to provide a comprehensive view of this event.

2.1. ZTF Optical Photometry

The ZTF differential point-spread-function (PSF) photometry of AT2022dbl is obtained through the ZTF Forced-Photometry Service (Masci et al. 2019). We clean the photometry results by filtering out epochs that are impacted by bad pixels, and requiring thresholds for the signal-to-noise ratio of the observations, seeing, zeropoint, the sigma-per-pixel in the input science image, and the 1- σ uncertainty on the difference image photometry measurement. We perform the baseline correction by the following two steps. First, we classify the measurements by the field, charge-coupled device (CCD) and quadrant identifiers. Then, for each class, we set the median of pre- or sufficiently post-flare counts as the offset. After that, we build the ZTF g - and r - band light curves for AT2022dbl. AT2022dbl was first alerted by ZTF in March 2018 and got the internal name ZTF18abdajx, and reported to TNS as AT2018mac. However, we carefully examine the light curves and confirm a false alert, which may be a temporary problem during the early test of ZTF.

2.2. ATLAS & ASAS-SN Optical Photometry

We obtain the ATLAS differential photometry from the ATLAS forced photometry server (Shingles et al. 2021). To improve the signal-to-noise ratio (SNR), we combine the data into 1-day bins and build the ATLAS c - and o -band light curves. Meanwhile, we obtain ASAS-SN differential photometry from the ASAS-SN sky patrol (Shappee et al. 2014; Kochanek et al. 2017). The Galactic extinction corrected light curves are shown in Figures 2(a) and (b).

2.3. LCO Optical Photometry

From January 22, 2024 to January 31, 2024, we conducted optical monitoring using the Las Cumbres Observatory Global Telescope network (LCOGT; Brown et al. 2013) in the u -, g -, r - and i -band with daily cadence. With the same method of Zhu et al. (2023), we use PanSTARRS (Flewelling

et al. 2020) *gri* band stack images as reference images and employ HOTPANTS (Becker 2015) for image subtraction. After image subtraction, we perform PSF photometry on the difference image, and the photometric results are calibrated using PS1 standards in the field of view. The Galactic extinction corrected photometric measurements are plotted in Figure 2(b).

2.4. Gaia, CRTS & PTF Optical Photometry

To check historical variability, we query the Gaia Photometric Science Alerts and the Catalina Real-Time Transient Survey (CRTS) (Drake et al. 2009) and Palomar Transient Facility (PTF) catalogs. To improve SNR, we combine the CRTS and PTF data into 10-day bins. The results are displayed and discussed in Section 3.2.1.

2.5. Swift UVOT & XRT Observations

The previous flare was fortunately well covered by Swift observations. During the previous flare, observations were performed by the X-Ray Telescope (XRT; Burrows et al. 2005) and the Ultra-Violet/Optical Telescope (UVOT; Roming et al. 2005) on Swift under a great number of ToO requests (Obs. ID: 00015026001-00015026045; PIs: Arcavi/Hinkle/Jiang/Makrygianni/Holoien/Margutti). The recent flare had been well followed under several ToO requests (Obs. ID: 00015026046-00015026064; PIs: Lin/Hammerstein), before Swift unfortunately entered the safe mode on March 15, 2024. We retrieve the Swift data from HEASARC¹ and process all data with `heasoft` v6.30.1. Details are described below.

For each UVOT epoch, we first examine each image file and exclude the extensions with bad photometric flags. For image files with multiple valid extensions, we sum all extensions using the task `uvotimsum`. Then, the task `uvotsource` performs photometry on each image, with the source and source-free background region defined by a circle of the radius of 20'' and 40'', respectively. The reference epochs are selected as those between MJD 60000 and 60300, which are late enough for the first flare to dissipate, and still well before the rise of the second flare.

For each XRT epoch, we reduce the data by `xrtpipeline` and obtain the level 2 products. Then we use `xrtproducts` to extract the level 3 products. After that, we use `xselect` to stack all images. On this stacked image, no discernible source is shown at the position of the transient. To obtain an upper limit, the source region is selected as a circle of radius 20'', while the background region is defined as a source-free annulus with an inner radius of 50'' and an outer radius of 150''. We obtain the source and background photon counts in 0.3-10 keV by `ximage`. For

images with photon counts in the source region $N \leq 80$, a Bayesian approach is applied to calculate the 3- σ lower and upper limits (Kraft et al. 1991); While for $N > 80$, a Gaussian approach is adopted (Evans et al. 2007, 2009; König et al. 2022). Based on single-epoch photometric results, we divide all epochs into four segments: (1) Epochs before MJD 59900. All of the results are upper limits, so we stack all images to get a tighter upper limit. The total exposure time is 78.7 ks. (2) Epochs between MJD 60000 and 60030. The two epochs are isolated from the others; one of them yields a weak detection with SNR ~ 2 . The total exposure time is only 2.3 ks. (3) One epoch on MJD 60235. It is just before the rise of the second flare (MJD ~ 60310), with an exposure time of 4.15 ks. (4) Since MJD 60310. Only one epoch reveals weak detection with SNR ~ 2 , and the total exposure time is 34.7 ks. The X-ray light curve is displayed in Figure 2(c).

2.6. Optical Spectroscopy

Since the discovery of the recurrent flare, we have obtained two spectra using the Double Spectrograph (DBSP; Oke & Gunn 1982) on the 200 inch Hale telescope at the Palomar Observatory (P200), and two spectra using the Himalaya Faint Object Spectrograph (HFOSC) instrument mounted on the 2-m Himalayan Chandra Telescope (HCT) of the Indian Astronomical Observatory (IAO, Prabhu 2014). The spectroscopic data are reduced in a standard manner using the packages in IRAF with the aid of the Python scripts hosted at REDPIPE (Singh 2021). We use `pypeit` package (Prochaska et al. 2020) to reduce the P200/DBSP spectra, and extract the HCT spectra by IRAF. As we retrieve the LCO photometric data, we find 12 automatically reduced public spectra taken by the 2.0m telescope at Haleakala Observatory, during the previous flare (Proposals: CON2022A-007/HAW2022A-002). We use 3 high-quality representative spectra of them, which are introduced and analyzed in Section 3.3.

2.7. WISE MIR Photometry

AT 2022dbl has been continuously observed by the Wide-field Infrared Survey Explorer (WISE; Wright et al. 2010), and the successive Near Earth Object Wide-field Infrared Survey Explorer (NEOWISE; Mainzer et al. 2011, 2014), at W1 (3.4 μm) and W2 (4.6 μm) bands every half year.

To check the potential MIR dust echo (Jiang et al. 2016; van Velzen et al. 2016), we query and download the W1- and W2-band photometric data from the AllWISE Multi-epoch Photometry Table and the NEOWISE-R Single Exposure (L1b) Source Table. We filter out the bad data points that have NaN magnitudes and errors; or get affected by a nearby image artifact (`cc_flags` $\neq 0$), the scattered moon light (`moon_masked` $\neq 0$), or a nearby detection (`nb` > 1). The

¹ <https://heasarc.gsfc.nasa.gov/cgi-bin/W3Browse/swift.pl>

remaining data points are grouped into approximately half-year bins to enhance the signal-to-noise ratio. No variability has been detected in the four epochs since the rise of the previous flare (MJD ~ 59706 – 60279). The averaged W1–W2 Vega magnitude for the host galaxy is 0.007 ± 0.006 . This result is consistent with Jiang et al. (2021), which found that most optical TDEs show very weak IR echoes likely due to a very low dust covering factor.

2.8. Radio Observations

According to Sfaradi et al. (2022)², on February 26, 2022 (around the peak of the previous flare), a 2-hour VLA observation revealed a single faint point source with flux density of $32 \pm 7 \mu\text{Jy}$ in the Ku-band ($\nu \sim 15$ GHz). The distance is ~ 0.4 arcsec from the reported position of AT 2022dbl, which is consistent with the position of the center of the host galaxy. However, the data are not publicly available.

Furthermore, the position of AT 2022dbl has also been observed by the Very Large Array Sky Survey (VLASS, Lacy et al. 2020) for three times. Two of the observations were performed before the flare: Epoch 1.1 on November 20, 2017 and Epoch 2.1 on August 1, 2020. The other is Epoch 3.1 on February 4, 2023, which was taken ~ 1 year after the peak of the previous flare. We retrieve tables and cutouts from the VLASS quick look catalog from CIRADA³, and confirm that no source has been detected within a radius of $1'$ in all three epochs. Hence, we shall not discuss the radio properties in the following texts.

3. DATA ANALYSIS

3.1. Host Galaxy

There exists an SDSS spectrum for the host galaxy SDSS J122045.04+493304.6. According to the `SpecObj` table, the redshift is $z = 0.02840 \pm 0.00001$, and the velocity dispersion $\sigma = 60.00 \pm 5.11 \text{ km s}^{-1}$. Using the relation of Kormendy & Ho (2013), we derive a black hole mass of $\log(M_{\text{BH}}/M_{\odot}) = 6.19 \pm 0.37$.

According to the `stellarMassStarformingPort` table, the stellar mass is $\log(M_{*}/M_{\odot}) = 9.88_{-0.25}^{+0.35}$. Using the $M_{*} - M_{\text{BH}}$ relation of Reines & Volonteri (2015), we derive a black hole mass of $\log(M_{\text{BH}}/M_{\odot}) = 6.31_{-0.41}^{+0.44}$, which is consistent with that derived from velocity dispersion.

The spectrum displays Balmer absorption line series of $\text{H}\alpha$, $\text{H}\beta$, $\text{H}\gamma$ and $\text{H}\delta$. According to the `galSpecLine` table, the equivalent width (EW) of $\text{H}\alpha$ emission line is $0.016 \pm 0.130 \text{ \AA}$. According to the `galSpecIndx` table, the Lick $\text{H}\delta_{\text{A}}$ index is $2.20 \pm 0.58 \text{ \AA}$. This agrees with the criteria of the quiescent Balmer-strong galaxy: $\text{H}\alpha \text{ EW} > -3 \text{ \AA}$ and $\text{H}\delta_{\text{A}} > 1.31 \text{ \AA}$ (French et al. 2016).

3.2. UV/Optical Photometric Analysis

3.2.1. Historical Variability

To check if there was any variability before the 2022 outburst, we first query the differential photometric data of ZTF (g and r bands), ATLAS (c and o bands) and ASAS-SN (g and V bands), as mentioned in Section 2.1 and 2.2. In addition, we query the Gaia Photometric Science Alerts (G band) and archival CRTS (V band) and PTF (R band) catalogs, as introduced in Section 2.4. In addition, we query the AllWISE and NEOWISE catalogs (MIR bands W1 and W2), and reduce the data using the method described in Section 2.7. The reduced light curves are displayed in Figure 1. Before this outburst, there is no significant variability except for a potential flare, which is only shown in the ASAS-SN light curve at MJD ~ 56600 (in 2013), ~ 970 rest-frame days before the first peak. Although the peak magnitude is comparable to the 2022 outburst, it is just above the detection limit of ASAS-SN, and it is not included in the ASAS-SN transient list⁴. More importantly, no contemporary photometric or spectroscopic data can determine whether it is related to the recent nuclear outbursts or caused by a nearby supernova outburst, considering the large FWHM of $\sim 16''$ for ASAS-SN (Jayasinghe et al. 2018, see also⁵). Therefore, we will not discuss this potential flare in the following text. For convenience, we refer to the flare that rose in 2022 as the “first flare,” and the flare that rose in 2024 as the “second flare.”

3.2.2. Light Curve Fitting

The optical/UV light curves during the first flare are displayed in Figure 2(a). The rise stage of the first flare is well covered by the ATLAS o band. Since the peak, the light curves are well covered by the Swift UVOT observations, and the first epoch happens to be around the peak. Therefore, we set the peak time to the first Swift epoch $t_{\text{peak1}} = (\text{MJD}) 59637.6$. For the UV/optical light curves since the peak, we use the `Superbol` package (Nicholl 2018) to interpolate the light curves and fit all photometry at each Swift epoch into a blackbody SED. The best-fit results are displayed in Figure 3. The blackbody temperature T_{bb} slowly declines from $\sim 3 \times 10^4 \text{ K}$ to $\sim 2 \times 10^4 \text{ K}$. The blackbody radius T_{bb} smoothly declines from $\sim 4 \times 10^{14} \text{ cm}$ to $\sim 1 \times 10^{14} \text{ cm}$.

The optical/UV light curves during the second flare are displayed in Figure 2(b). Its rise stage is well covered by the ZTF and LCO g band. We choose the peak time as the brightest Swift epoch, $t_{\text{peak2}} = (\text{MJD}) 60346.6$, and perform the blackbody fitting on all photometry at Swift epochs except for the last one, which is apparently problematic. As shown in Figure 3, from -15 d to $+30 \text{ d}$, the blackbody temperature

² <https://www.wis-tns.org/astronotes/astronote/2022-57>

³ <https://cirada.ca/vlascatalogueql0>

⁴ <https://www.astronomy.ohio-state.edu/asassn/transients.html>

⁵ <https://www.astronomy.ohio-state.edu/asassn/public>

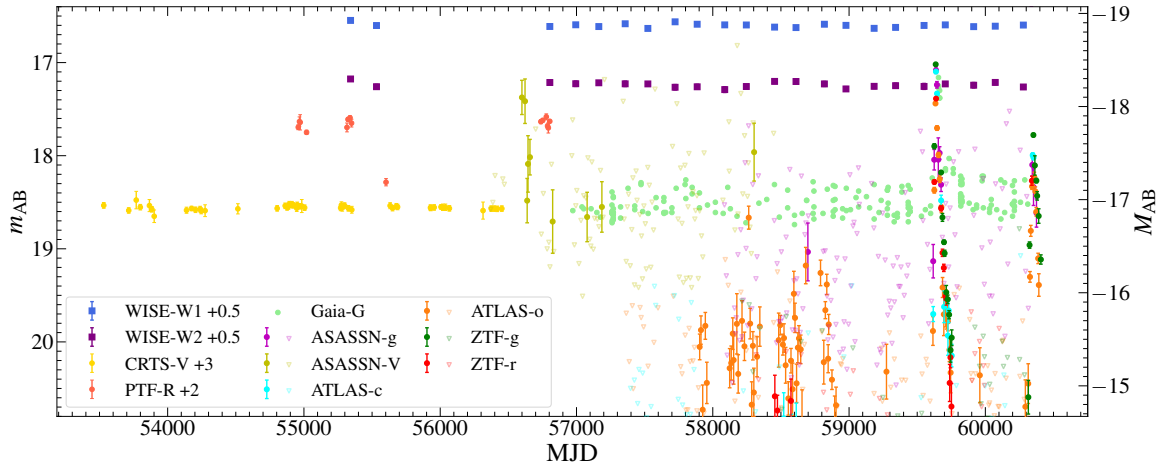


Figure 1. The historical light curves of the position of AT 2022dbl. We collect the optical photometric data after subtracting the host contributions from ZTF in the g and r bands, from ATLAS in the c and o bands, and from ASAS-SN in the g and V bands. Additionally, we compile optical photometry from CRTS in the V band, PTF in the R band, and Gaia in the G band, along with the WISE mid-infrared (MIR) photometry in the $W1$ and $W2$ bands. To improve the signal-to-noise ratio, we binned the data into 10-day bins for all optical bands except for Gaia- G , and into approximately half-year bins for the MIR bands $W1$ and $W2$.

remains fairly constant at ~ 26000 K, while the blackbody luminosity evolves slowly, peaking ~ 0.4 dex lower than the previous flare. Although the flat peak has been well covered by Swift, it has unfortunately entered safe mode since March 15, 2024, which was exactly when the source left the peak. After that, the decline stage is sparsely covered by the ZTF g and ATLAS o bands.

We characterize the light curves of both flares by the rest-frame rise time from half-peak luminosity to peak luminosity ($t_{1/2,\text{rise}}$) and the decline time from peak luminosity to half-peak luminosity ($t_{1/2,\text{decline}}$). To extract these two timescales, we fit the light curves with a Gaussian rise and a power-law decline:

$$L(t) = L(t_{\text{peak}}) \times \begin{cases} e^{-(t-t_{\text{peak}})^2/(2\sigma^2)}, & t < t_{\text{peak}}; \\ \left(\frac{t-t_{\text{peak}}+\tau}{\tau}\right)^\alpha, & t \geq t_{\text{peak}}. \end{cases} \quad (1)$$

For the first flare, the rise and decline fittings are performed on the o -band and blackbody luminosity, respectively. For the second flare, the fitting is performed on the g -band luminosity. The best-fitted light curves are drawn in the top panel of Figure 3, and the fitted parameters are listed in Table 1.

3.3. Optical Spectral Analysis

As introduced in Section 2.6, 3 LCO spectra taken during the first flare were selected, while 4 optical spectra have been taken during the second flare. In addition, an SDSS host spectrum is available. All of these spectra are shown in Figure 4. The spectral fitting procedures for each transient spectrum are listed as follows:

(1) Host-galaxy subtraction. Since the host spectrum displays clear Ca II absorption doublets at 3910–4000 Å, and

the blue side has higher SNR than the red side, we used these doublets for calibration. We fit and subtract the nearby pseudo-continuum for both the transient and host spectra. Then a least-squares fitting on the residuals gives the multiplication factor for the host galaxy component. Limited by the wavelength range of the host spectrum, we perform the fitting only within this range. The three representative LCO spectra were taken at MJD 59638 (+0 d), MJD 59664 (+26 d) and MJD 59690 (+51 d). The two HCT spectra taken at the early stage of the second flare are discarded, as their SNRs are too low for the host-galaxy subtraction and also for further analysis.

(2) Continuum fitting. After subtracting the host component, a power-law function is used to fit the continuum. In the case of LCO spectra, the continuum windows are set to the following line-free regions (in rest-frame wavelengths): 3700–3900 Å, 5200–5400 Å, 6100–6300 Å, 7100–7400 Å and 7600–8490 Å, with the exclusion of the telluric absorption regions. For the P200 spectra, the continuum and telluric absorption regions are a bit different (see Figure A1).

(3) Line fitting. After subtracting the continuum, all residuals exhibit multiple broad characteristics around 3900–4200 Å, 4400–5200 Å, and 6300–6900 Å, some showing a faint broad bump around 5500–6100 Å. The broad feature in the 3900–4200 Å range is symmetrical and peaks at approximately 4100 Å, possibly corresponding to N III (4100) or H δ (4101). In the range 4400–5200 Å, the characteristic is asymmetric and could be a combination of N III (4640), He II (4686) and H β (4861). Lastly, the broad feature in the range 6300–6900 Å is symmetric and centers around 6560 Å. It is consistent with a broad H α (6563) emission line; The 5500–6100 Å feature can be tentatively interpreted as He I (5876). The selection of the fitting components is based on

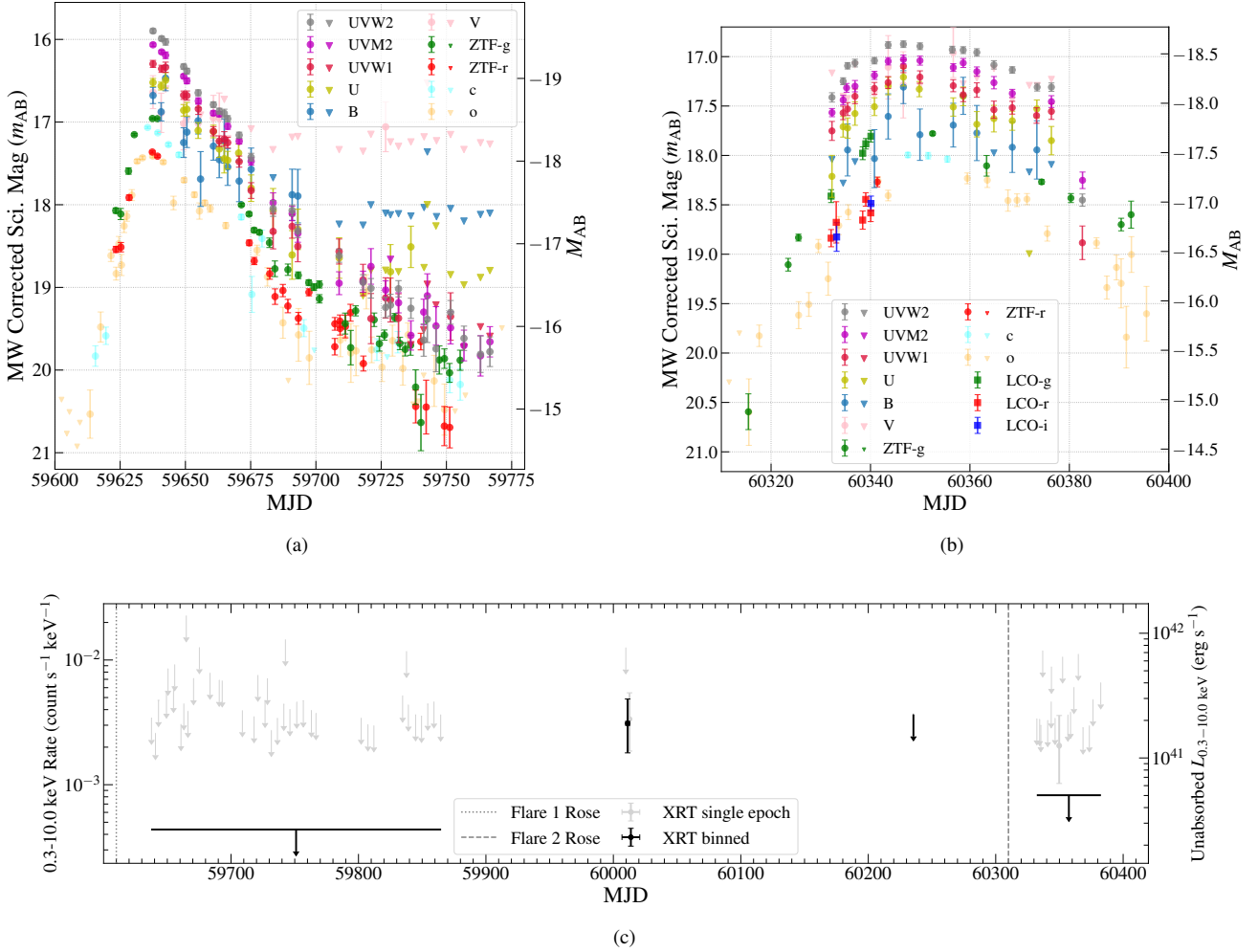


Figure 2. (a) and (b): The UV/optical light curves of AT 2022dbl during the first and the second flare, respectively. $3-\sigma$ upper limits are plotted in down triangles. **(c):** The X-ray count rate of AT 2022dbl. The vertical dotted and dashed lines mark the approximate rise time of the first and second flares, respectively. $3-\sigma$ upper limits are plotted in down arrows.

these facts: First, the extended red wing of the 4400–5200 Å feature indicates the existence of $H\beta$, which is further supported by the existence of $H\alpha$. Second, it is unlikely that the 3900–4200 Å bump is dominated by $H\delta$, since $H\alpha$ is too weak compared to this feature. Therefore, it should be dominated by N III (4100), although the $H\delta$ will slightly affect the intensity. The N III $\lambda 4100$ lines are usually produced by the Bowen mechanism, which requires He II Ly α lines at 304 Å. Taking into account the extreme strength of N III $\lambda 4100$, the He II emission should be strong. Moreover, the N III $\lambda 4640$ lines should also be produced via this mechanism. Therefore, both the He II $\lambda 4686$ line and the N III $\lambda 4640$ line should be considered. In addition, a He I $\lambda 5876$ component is involved to cover the weak emission features in several spectra. To ensure reliability, the FWHM and the offset of the two features of N III, as do those of $H\alpha$ and $H\beta$. The fitting results are shown in Figure A1.

Despite careful selection of fitting components, the 4400–5200 Å feature is still hard to deblend due to its smoothness, and hence it cannot prove or disprove the existence of He II $\lambda 4686$ and the associated Bowen mechanism as well as the intensity of N III $\lambda 4640$. Therefore, we only focus on the evolution of the most prominent and unblended features: N III $\lambda 4100$ and $H\alpha$. Furthermore, we also examine the power-law indexes of the continua. Figure 5 illustrates the evolution of the FWHM, velocity shift and luminosity of N III $\lambda 4100$ and $H\alpha$ emission lines, along with the power-law indexes of the continua, during both flares.

For the LCO spectra taken during the first flare, the FWHMs for the $H\alpha$ lines in all spectra are well above 10000 $km s^{-1}$, showing a slowly narrowing trend from FWHM $\sim 18000 km s^{-1}$ to $\sim 12000 km s^{-1}$ during +0 d to +51 d to the first peak. N III $\lambda 4100$ shows a narrowing trend from FWHM $\sim 12000 km s^{-1}$ to $\sim 9000 km s^{-1}$. Except for the first epoch, neither of the N III $\lambda 4100$ lines nor $H\alpha$ exhibit clear shifts

Table 1. The best-fitted light curve parameters for the two flares

Flare	t_{peak}	$L_{\text{BB,peak}}$	$T_{\text{BB,peak}}$	$R_{\text{BB,peak}}$	$t_{1/2,\text{rise}}$	$t_{1/2,\text{decline}}$	E_{bol}
[No.]	[MJD]	[log (erg s ⁻¹)]	[10 ⁴ K]	[10 ¹⁴ cm]	[day]	[day]	[log (erg)]
1	59637.6	43.89 ± 0.10	2.91 ± 0.19	3.87 ± 0.31	10.6 ± 0.5	15.7 ± 0.8	50.4
2	60346.6	43.48 ± 0.12	2.64 ± 0.23	2.92 ± 0.34	16.8 ± 0.5	36.9 ± 2.4	50.2

NOTE— $t_{1/2,\text{rise}}$: the rest-frame rise time from half-peak luminosity to peak luminosity.
 $t_{1/2,\text{decline}}$: the rest-frame decline time from peak luminosity to half-peak luminosity.
 E_{bol} : Bolometric energy from rest-frame -50 d to +100 d.

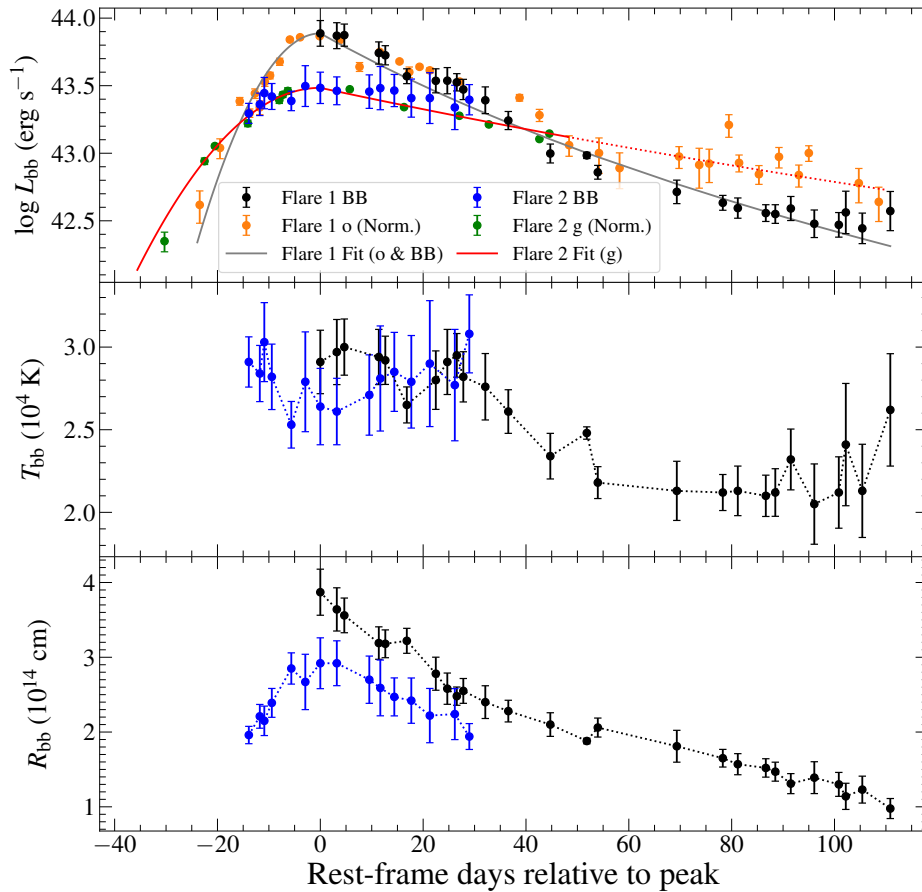


Figure 3. The light curve fitting results of AT 2022dbl. The luminosities of the *o*- and *g*-bands are normalized to the blackbody luminosities of the first and second flares, respectively. For comparison, the fitted decline curve for the second flare is extended to $\sim +120$ d in the dotted style.

towards blue or red. The luminosity of H α and N III $\lambda 4100$ gets lower at later phases. The high N III $\lambda 4100$ luminosity of $\sim 10^{41}$ erg s⁻¹ and the evolution of N III $\lambda 4100$ / H α ratio highly resemble AT2018dyb, which has the highest N III $\lambda 4100$ luminosity among spectroscopically confirmed TDEs (Leloudas et al. 2019; Charalampopoulos et al. 2022). We note that the precision of the luminosity depends on the flux calibration. The continuum gets flatter as it gets fainter.

For the first P200 spectrum (-6 d to the second peak), it displays an H α emission line with FWHM ~ 10000 km s⁻¹ and N III $\lambda 4100$ with FWHM ~ 13000 km s⁻¹, while the velocity shift and luminosity for both lines are similar to the late-time spectra of the previous flare. The power-law index for the continuum rises again, which is consistent with a newly risen flare. The second P200 spectrum displays a much narrower and weaker H α feature with FWHM ~ 4000 km s⁻¹ and a luminosity of $< 10^{40}$ erg s⁻¹, which fades much

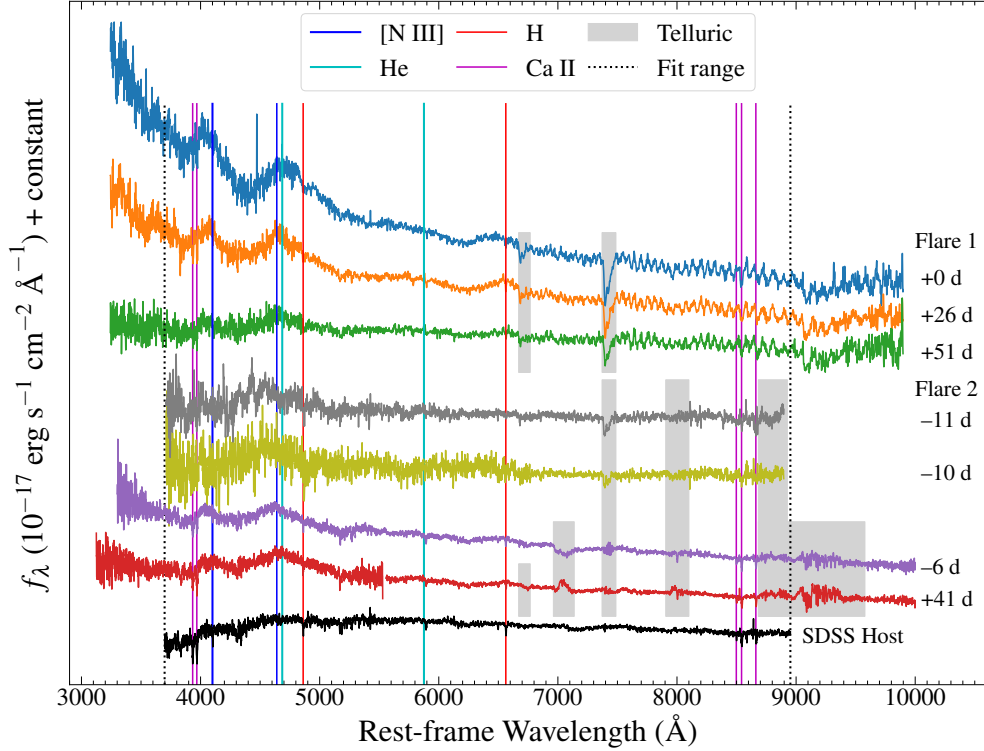


Figure 4. The optical spectra of AT 2022dbl. Black dotted lines limit the range of the spectral fitting.

quicker than the N III $\lambda 4100$ feature. As a result, the ratio N III $\lambda 4100 / H\alpha$ increases to $\gtrsim 1$. The power-law index for the continuum is higher than that of the previous spectrum.

3.4. X-ray Analysis

As described in Section 2.5, X-ray observations were made with Swift XRT during both flares. All X-ray epochs are divided into four segments, as shown in Figure 2(c). Only one segment yields a marginal detection with an $\text{SNR} \sim 2$, which does not allow for spectral analysis. The stacked image of the first phase (+0 d to +220 d to the first peak) yields a total exposure time of 78.7 ks and a tight $3\text{-}\sigma$ upper limit for the 0.3–10.0 keV count rate of 4.37×10^{-4} counts s^{-1} . Assuming a power-law index of $\Gamma = 3$ and a hydrogen column density of $N_{\text{H}} = 1.94 \times 10^{20}$ cm^{-2} (HI4PI Collaboration et al. 2016), we obtain an upper limit for the unabsorbed luminosity using the WebPIMMS tool⁶ of $L_{\text{X},1} < 2.7 \times 10^{40}$ erg s^{-1} . Following the same method, we derive the luminosity for the later three segments: $L_{\text{X},2} = 1.9_{-0.8}^{+1.1} \times 10^{41}$ erg s^{-1} , $L_{\text{X},3} < 2.2 \times 10^{41}$ erg s^{-1} , $L_{\text{X},4} < 5.0 \times 10^{40}$ erg s^{-1} .

4. DISCUSSION

4.1. AT 2022dbl as a robust repeated pTDE

We shall discuss the origin of these two flares as follows. The pre-outburst SDSS spectrum exhibits a series of strong

Balmer absorption lines that are in accordance with a quiescent Balmer-strong galaxy with no sign of AGN activity. This strongly disfavors the presence of a persistent AGN. In addition, the first flare lasted less than a year, which is unusual for a turn-on AGN, and the second flare showed a number of similar photometric and spectroscopic features. We thereby reject the possibility of an AGN origin for both flares. On the other hand, both flares show broad $H\alpha$ emission with $\text{FWHM} > 10000$ km s^{-1} and declining blackbody radii after the peak, which also strongly contradicts the SN origin.

All of the features that disfavour AGNs and supernovae are nevertheless characteristic of TDEs, including the timescales of both flares, the fairly steady blackbody temperatures of $(2-3) \times 10^4$ K, the value and evolution of the blackbody radii, and the very broad $H\alpha$ emission. Therefore, AT 2022dbl is undoubtedly a repeated TDE. Moreover, both flares display highly similar broad $H\alpha$, $\sim 4400\text{--}5200$ \AA ($H\beta$ & possible N III and He II) and ~ 4100 \AA (N III & possible $H\delta$) features, as shown in Figure 6. In particular, for both flares, the luminosity of ~ 4100 \AA is comparable to that of $H\alpha$ (See the lower left panel of Figure 5), which is rare among all TDEs. Hence, these two flares are probably originated from the debris of a single disrupted star, and AT 2022dbl should be a robust repeated pTDE.

We now try to rebuild the orbit of this "unluckiest star", before it got stripped by the BH. Assuming a BH mass of $10^{6.19} M_{\odot}$, and an elliptical orbit with a period of ~ 710 days, the semi-major axis of the orbit should be $\log a$ (cm) = 15.4,

⁶ <https://heasarc.gsfc.nasa.gov/cgi-bin/Tools/w3pimms/w3pimms.pl>

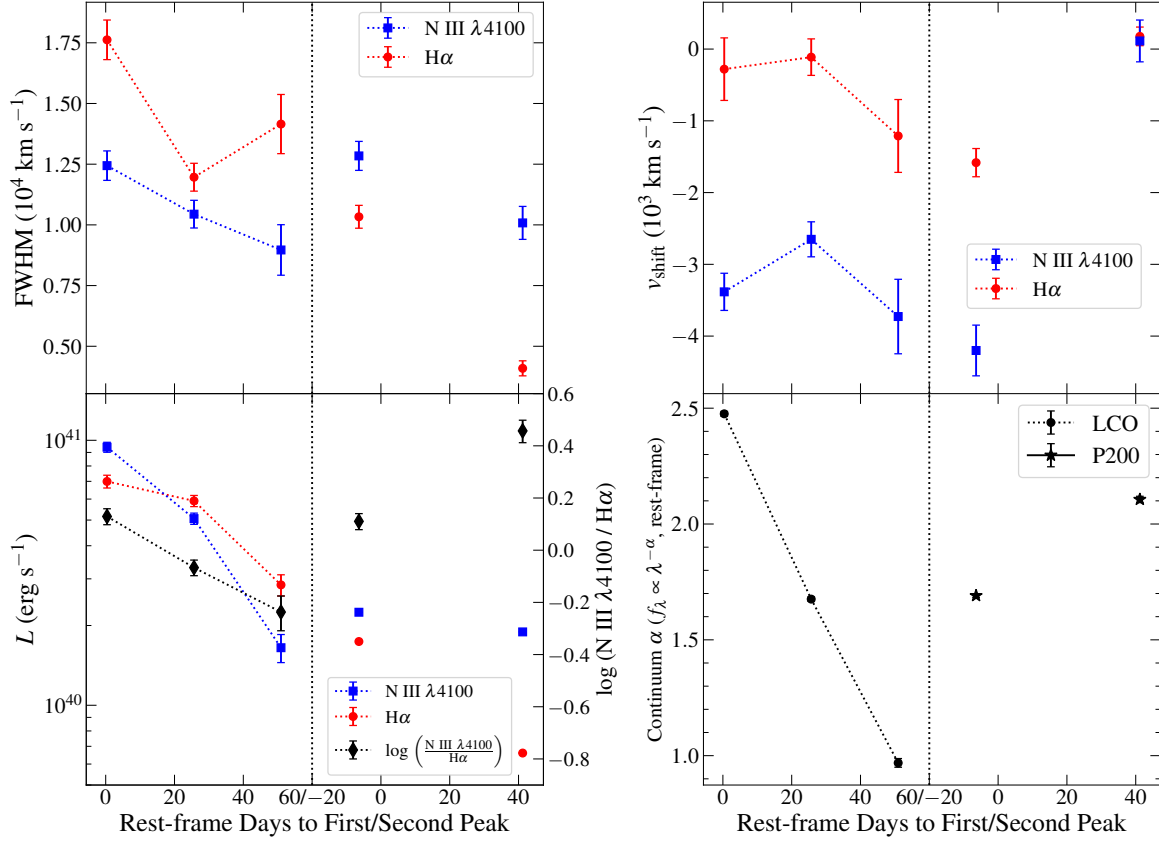


Figure 5. The evolution of the FWHM, velocity shift and luminosity of N III $\lambda 4100$ (blue squares) and H α (red dots) emission lines as well as their ratios (black diamonds), and the power-law indexes of the continua. In the last panel, measurements from the LCO spectra taken during the first flare and P200 spectra taken during the second flare are marked in dots and asterisks, respectively.

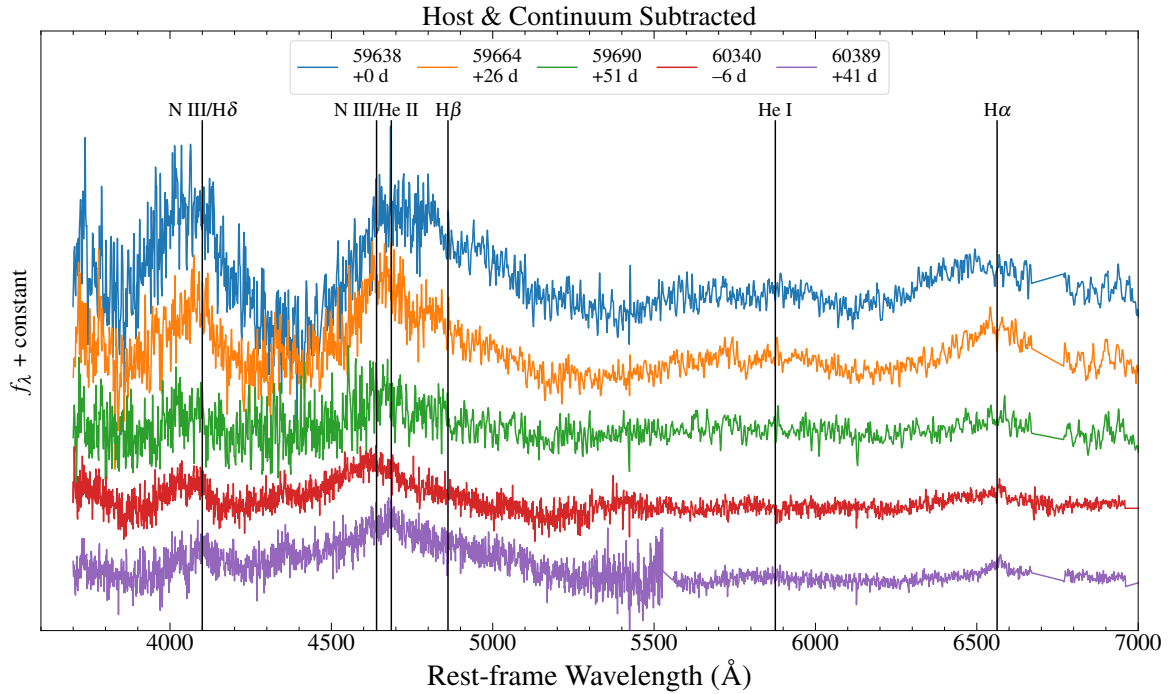


Figure 6. Spectra after subtracting the host galaxy contribution and the continuum. Spectra of both flares show similar emission lines.

or $a \approx 180$ AU. For a solar-like star, the tidal radius should be $\log R_t$ (cm) = 12.9, or $R_t \approx 0.5$ AU. Hence, the eccentricity

is $e = 1 - R_p/a \sim 1 - R_t/a \approx 0.997$. Both the eccentricity and the BH mass are well consistent with the pTDE scenario of Lu & Quataert (2023): Flares are produced by the unstable mass transfer due to Roche lobe overflow of a low-mass main sequence star in a highly eccentric ($e \gtrsim 0.95$) orbit around a BH with mass $\gtrsim 10^6 M_\odot$, after the Hills breakup of a stellar binary into a hypervelocity star and a bound star.

4.2. Comparison with other repeated pTDEs and common optical TDEs

As mentioned in Section 1, several repeated pTDEs have been reported in the literature: ASASSN-14ko, eRASST J045650.3–203750, AT2018fyk, RX J133157.6–324319.7 and AT 2020vdq. We briefly list the information of these repeated pTDEs in Table 2.

As shown in the table, only ASASSN-14ko, AT 2020vdq and AT 2022dbl show recurring flares in optical bands. We only focus on the comparison of AT 2020vdq and AT 2022dbl, as they share similar intervals and host galaxy types, while the behavior of ASASSN-14ko differs greatly. We compare the peak blackbody luminosity and radius, the bolometric energy and the rise and decline timescales of AT 2022dbl with those of AT 2020vdq and other ZTF TDEs listed in Yao et al. (2023), as plotted in Figure 7.

AT 2022dbl shows several differences compared to AT 2020vdq. First, its peak luminosity for the second flare is ~ 0.4 dex lower than that of the first flare; While for AT 2020vdq, the peak luminosity of the second flare is ~ 1.2 dex higher than that of the first flare. Second, for AT 2022dbl, the bolometric energy of the second flare is only ~ 0.2 dex lower than that of the first flare, as the second flare rises and declines slower than the first flare. In contrast, for AT 2020vdq, the second flare rises and declines much more quickly than the first flare, reducing the difference between the bolometric energy of the second flare and the first flare to ~ 0.7 dex.

We compare AT 2020vdq and AT 2022dbl with the ZTF TDEs (Yao et al. 2023) that show no recurrence flare by now. For AT 2020vdq, the peak luminosity and the bolometric energy of its first flare are the lowest and the second lowest among all optical TDEs, while the rise and decline timescales of its second flare are the lowest and the second lowest among all optical TDEs. In short, both flares of AT 2020vdq show some peculiarities compared to normal TDEs. For AT 2022dbl, its peak blackbody radius is the smallest among all TDEs with $6 \leq \log(M_{\text{BH}}/M_\odot) \leq 7$. Apart from this, its peak luminosity, bolometric energy, rise and decline timescales of both flares are all typical among optical TDEs. Therefore, the two flares of AT 2022dbl are

not significantly different from the ZTF TDEs, implying that some pTDEs may be hidden in the ZTF sample.

4.3. Robustness of a "repeated pTDE" classification

As introduced in Section 1, the identification of a repeated pTDE can be complicated by some alternative origins. Hence, a robust identification of a repeated pTDE (especially an optical one) is difficult. It requires not only confirmation of the TDE origin but also a trustworthy connection between the flares.

As an example, we examine the case of AT 2020vdq. In Somalwar et al. (2023a), the authors establish the TDE origin for the first flare by the broadband light curve, the newly risen radio flare, the E+A host galaxy, as well as the intermediate width ($\sim 700\text{--}1000 \text{ km s}^{-1}$) Balmer, He II, He I, and [Fe X] emission in the late-time spectra ($\sim +600$ d). In Somalwar et al. (2023b), the second flare is spectroscopically identified as a TDE, since the spectra around the peak exhibit broad ($\sim 20000 \text{ km s}^{-1}$) Balmer, He II and He I emission lines. Although the TDE-H+He identification for both flares is reliable, the two flares show highly different peak luminosity and light curve shapes and have no contemporary spectra to support their physical connection. Moreover, the E+A host galaxy may have a much higher TDE rate than normal galaxies (Arcavi et al. 2014; French et al. 2016; Hammerstein et al. 2021). In an extreme case, the probability of detecting two independent TDEs within ~ 3 years can be as high as 30% (See Section 5.1 of Somalwar et al. 2023b). Therefore, we conclude that the classification of AT 2020vdq as a repeated pTDE remains to be determined in the future.

In the case of AT 2022dbl, its two flares not only exhibit photometric and spectroscopic features that firmly establish their TDE origins, but also display similar broad Balmer, N III, and possible He II emission lines in the early spectra of both flares, strongly indicating a connection between them (see Figure 6). This represents the first robust spectroscopic evidence for a repeated pTDE.

This spectroscopic evidence is important for the repeated pTDE classification, as current photometric data for both events cannot provide enough support. On the one hand, there are only two flares in both events, allowing for alternative origins, especially independent TDEs, as their host galaxies can have higher TDE rates than normal galaxies. On the other hand, although the light curves can provide additional information on the judgment of repeated pTDEs, there is currently lack of light curve model of repeated pTDEs or reliable optical/UV repeated pTDEs for comparison. A third flare can provide the conclusive evidence for a repeated pTDE classification, which might occur in the next couple of years.

As illustrated in Figure 7(b), for both events, their two flares share similar peak blackbody radius. The radius for

Table 2. List of published repeated pTDEs

Name	Host Type	Band	Period/Interval (Days)	Flares	Peak Evolution
ASASSN-14ko ^{1,2,3,4}	Seyfert 2	Opt./UV/X-ray [†]	115.2	~30	Similar
eRASSt J045650.3–203750 ^{5,6}	Quiescent	X-ray/UV [†]	299→193	5	Lower
AT2018fyk ^{7,8}	LINER/Retired	UV/X-ray	~1200	2	Lower
RX J133157.6-324319.7 ^{9,10}	Quiescent	X-ray	~10000	2	Similar
AT 2020v dq ^{11,12,13}	E+A	Opt./UV*/X-ray*	~870	2	Higher
AT 2022dbl ¹⁴	QBS	Opt./UV	~710	2	Lower

NOTE—

- Band: † Not periodic. * Not observed during the first flare.
- Period/Interval: Only ASASSN-14ko shows a nearly constant period of 115.2 days. eRASSt J045650.3–203750 is ongoing; it has shown 5 flares with the interval declining from 299 days to ~193 days. Other pTDEs show only two flares.
- Peak Evolution: The peak luminosity of the earlier flare versus that of the later flare.
- References: 1. Payne et al. (2021), 2. Payne et al. (2022), 3. Payne et al. (2023), 4. Huang et al. (2023), 5. Liu et al. (2023), 6. Liu et al. (2024), 7. Wevers et al. (2019), 8. Wevers et al. (2023), 9. Hampel et al. (2022), 10. Malyali et al. (2023), 11. Yao et al. (2023), 12. Somalwar et al. (2023a), 13. Somalwar et al. (2023b), 14. This work.

AT 2022dbl is $\log R_{\text{bb}}$ (cm) ~ 14.5 , which lies between the tidal radius, $\log R_t$ (cm) = 12.9 and the semi-major axis, $\log a$ (cm) = 15.4. This relation is also found in AT 2020v dq: $\log R_{\text{bb}}$ (cm) ~ 14.9 , $\log R_t$ (cm) = 12.7, $\log a$ (cm) = 15.3. This similarity provides additional support for a pTDE claim, as it suggests the connection between these two flares. Based on the relation, we tentatively propose this scenario: The star shallowly encounters the SMBH and loses a small fraction of mass, then leaves the tidal radius with the orbit largely unaffected. As a result, the bound debris can self-intersect at a similar radius, which is far away from both the pericenter and apocenter. Additional theoretical works and numerical simulations are encouraged to test this scenario.

5. CONCLUSION

We have reported the discovery of a repeated partial TDE AT 2022dbl in a nearby quiescent galaxy. In this event, two separate flares occurred in 2022 and 2024, with an interval of ~710 days. Both flares have been fortunately followed by high cadence optical/UV photometry and X-ray observations, as well as a series of optical spectroscopy observations, which help to confirm the TDE origin for both flares. More importantly, similar broad Balmer, N III and possible He II emission lines, especially the extreme ~4100 Å emission lines, help to rule out the possibility of two independent TDEs and provide the first robust spectroscopic evidence for two tidal disruptions of the same star.

AT 2022dbl is a clear example of an optical/UV repeated pTDE, as it emits the majority of its energy in the optical/UV wavelengths, at least in our line of sight. Repeated pTDEs, particularly optical/UV bright TDEs like AT 2022dbl, provide valuable opportunities to test optical/UV emission models, as another flare is expected in the coming years. Its re-

peatability enables us to carefully plan for multi-wavelength observations of subsequent flares from the earliest stages. With the assistance of high-cadence optical/UV/X-ray photometric and spectroscopic data, we may have the chance to uncover the final answer to the mechanism of optical/UV emission of TDEs, as well as the associated "missing energy" problem (Lu & Kumar 2018). As the next-generation "TDE hunters" come into play, such as the Vera Rubin Observatory (VRO; Ivezić et al. 2019) and the Wide Field Survey Telescope (WFST; Lin et al. 2022; Wang et al. 2023), the high-cadence multiband surveys are expected to reveal a number of such pTDEs and accelerate the process of solving these puzzles in the near future.

This work is supported by National Key Research and Development Program of China (2023YFA1608100), the National Natural Science Foundation of China (grants 12393814, 12233008, 12073025, 12192221), the Strategic Priority Research Program of the Chinese Academy of Sciences (XDB0550200, XDB41000000), the China Manned Space Project (No. CMS-CSST-2021-A13), the Fundamental Research Funds for Central Universities (WK3440000006) and the Anhui Provincial Natural Science Foundation (2308085QA32). K. M. acknowledges support from JSPS KAKENHI grant No. JP24H01810. The authors appreciate the support of the Cyrus Chun Ying Tang Foundations. We thank the Swift science operations team for accepting our ToO requests and arranging the observations. We thank all researchers who have submitted Swift ToO requests and LCO spectroscopy proposals. We thank the staff of IAO, Hanle, CREST, and Hosakote, who made these observations possible. The facilities at IAO and CREST are operated by the Indian Institute of Astrophysics, Bangalore. We thank

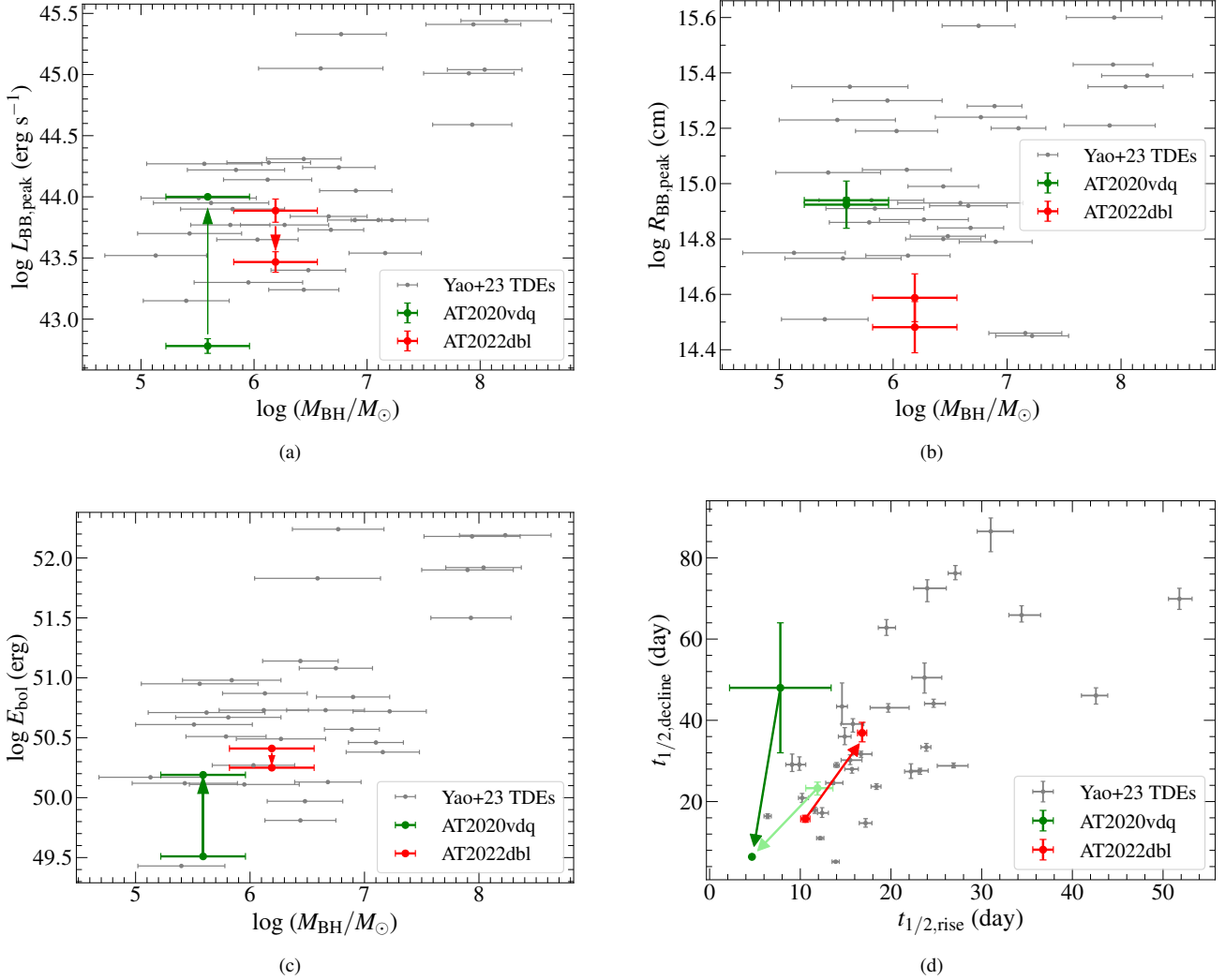


Figure 7. Comparison of optical repeated pTDEs AT 2020vdq (Yao et al. 2023; Somalwar et al. 2023b) and AT 2022dbl (This work), as well as optical TDEs listed in Yao et al. (2023). Black hole mass versus (a): Peak blackbody luminosity; (b): Peak blackbody radius; (c): Bolometric energy from -50 d to $+100$ d. (d): Rest-frame rise time from half-peak luminosity to peak luminosity versus decline time from peak luminosity to half-peak luminosity.

Note: (1) In Plot (b), both AT 2020vdq and AT 2022dbl show similar blackbody radius in their two flares. (2) Plot (c) is adapted from Figure 4 of the preprint of Somalwar et al. (2023b). However, we find some values in that figure are highly overestimated and recalculate them. (3) The parameters of AT 2020vdq are mostly adopted or derived from Somalwar et al. (2023b). However, in Plot (d), the derived rise and decline timescales of the first flare of AT 2020vdq in Yao et al. (2023) and Somalwar et al. (2023b) are greatly different, hence plotted in light-green and green, respectively.

Prof. Christoffer Fremling and Nicholas Earley for helping us obtain a P200 spectrum on March 20, 2024. We acknowledge the support of the staff of the Lijiang 2.4m telescope, although we failed to obtain a usable spectrum. ZL thanks Dr. Junbo Zhang, Dr. Jie Zheng and Dr. Junjie Jin for the kind help on the ToO observation on the Xinglong 2.16m telescope and the subsequent data reduction, and sincerely apologizes for not using this low-resolution spectrum. ZL sincerely thanks the UK Swift Science Data Centre (UKSSDC) helpdesk (especially Phil and Kim) for the kind instructions and *Swift* replies on the reduction of XRT data. ZL thanks

Robert Wiegand for the help on the reduction of UVOT data. The ZTF forced-photometry service was funded under the Heising-Simons Foundation grant #12540303 (PI: Graham). This research uses data obtained through the Telescope Access Program (TAP). Observations with the Hale Telescope at Palomar Observatory were obtained as part of an agreement between the National Astronomical Observatories, Chinese Academy of Sciences, and the California Institute of Technology.

APPENDIX

A. FITTING PLOTS FOR OPTICAL SPECTRA

REFERENCES

- Arcavi, I., Gal-Yam, A., Sullivan, M., et al. 2014, *ApJ*, 793, 38, doi: [10.1088/0004-637X/793/1/38](https://doi.org/10.1088/0004-637X/793/1/38)
- Becker, A. 2015, HOTPANTS: High Order Transform of PSF ANd Template Subtraction, Astrophysics Source Code Library, record ascl:1504.004. <http://ascl.net/1504.004>
- Bellm, E. C., Kulkarni, S. R., Graham, M. J., et al. 2019, *PASP*, 131, 018002, doi: [10.1088/1538-3873/aaecbe](https://doi.org/10.1088/1538-3873/aaecbe)
- Bortolas, E. 2022, *MNRAS*, 511, 2885, doi: [10.1093/mnras/stac262](https://doi.org/10.1093/mnras/stac262)
- Brown, T. M., Baliber, N., Bianco, F. B., et al. 2013, *PASP*, 125, 1031, doi: [10.1086/673168](https://doi.org/10.1086/673168)
- Burrows, D. N., Hill, J. E., Nousek, J. A., et al. 2005, *SSRv*, 120, 165, doi: [10.1007/s11214-005-5097-2](https://doi.org/10.1007/s11214-005-5097-2)
- Charalampopoulos, P., Leloudas, G., Malesani, D. B., et al. 2022, *A&A*, 659, A34, doi: [10.1051/0004-6361/202142122](https://doi.org/10.1051/0004-6361/202142122)
- Chen, J.-H., & Shen, R.-F. 2021, *ApJ*, 914, 69, doi: [10.3847/1538-4357/abf9a7](https://doi.org/10.3847/1538-4357/abf9a7)
- Cufari, M., Coughlin, E. R., & Nixon, C. J. 2022, *ApJL*, 929, L20, doi: [10.3847/2041-8213/ac6021](https://doi.org/10.3847/2041-8213/ac6021)
- Dai, L., McKinney, J. C., Roth, N., Ramirez-Ruiz, E., & Miller, M. C. 2018, *ApJL*, 859, L20, doi: [10.3847/2041-8213/aab429](https://doi.org/10.3847/2041-8213/aab429)
- Drake, A. J., Djorgovski, S. G., Mahabal, A., et al. 2009, *ApJ*, 696, 870, doi: [10.1088/0004-637X/696/1/870](https://doi.org/10.1088/0004-637X/696/1/870)
- Evans, P. A., Beardmore, A. P., Page, K. L., et al. 2007, *A&A*, 469, 379, doi: [10.1051/0004-6361:20077530](https://doi.org/10.1051/0004-6361:20077530)
- . 2009, *MNRAS*, 397, 1177, doi: [10.1111/j.1365-2966.2009.14913.x](https://doi.org/10.1111/j.1365-2966.2009.14913.x)
- Fitzpatrick, E. L. 1999, *PASP*, 111, 63, doi: [10.1086/316293](https://doi.org/10.1086/316293)
- Flewelling, H. A., Magnier, E. A., Chambers, K. C., et al. 2020, *ApJS*, 251, 7, doi: [10.3847/1538-4365/abb82d](https://doi.org/10.3847/1538-4365/abb82d)
- French, K. D., Arcavi, I., & Zabludoff, A. 2016, *ApJL*, 818, L21, doi: [10.3847/2041-8205/818/1/L21](https://doi.org/10.3847/2041-8205/818/1/L21)
- Gezari, S. 2021, *ARA&A*, 59, 21, doi: [10.1146/annurev-astro-111720-030029](https://doi.org/10.1146/annurev-astro-111720-030029)
- Guillochon, J., & Ramirez-Ruiz, E. 2013, *ApJ*, 767, 25, doi: [10.1088/0004-637X/767/1/25](https://doi.org/10.1088/0004-637X/767/1/25)
- Guo, H., Sun, J., Li, S.-L., et al. 2023, arXiv e-prints, arXiv:2312.06771, doi: [10.48550/arXiv.2312.06771](https://doi.org/10.48550/arXiv.2312.06771)
- Hammerstein, E., Gezari, S., van Velzen, S., et al. 2021, *ApJL*, 908, L20, doi: [10.3847/2041-8213/abdcb4](https://doi.org/10.3847/2041-8213/abdcb4)
- Hammerstein, E., van Velzen, S., Gezari, S., et al. 2023, *ApJ*, 942, 9, doi: [10.3847/1538-4357/aca283](https://doi.org/10.3847/1538-4357/aca283)
- Hampel, J., Komossa, S., Greiner, J., et al. 2022, *Research in Astronomy and Astrophysics*, 22, 055004, doi: [10.1088/1674-4527/ac5800](https://doi.org/10.1088/1674-4527/ac5800)
- HI4PI Collaboration, Ben Bekhti, N., Flöer, L., et al. 2016, *A&A*, 594, A116, doi: [10.1051/0004-6361/201629178](https://doi.org/10.1051/0004-6361/201629178)
- Hills, J. G. 1975, *Nature*, 254, 295, doi: [10.1038/254295a0](https://doi.org/10.1038/254295a0)
- . 1988, *Nature*, 331, 687, doi: [10.1038/331687a0](https://doi.org/10.1038/331687a0)
- Huang, S., Jiang, N., Shen, R.-F., Wang, T., & Sheng, Z. 2023, *ApJL*, 956, L46, doi: [10.3847/2041-8213/acffc5](https://doi.org/10.3847/2041-8213/acffc5)
- Ivezić, Ž., Kahn, S. M., Tyson, J. A., et al. 2019, *ApJ*, 873, 111, doi: [10.3847/1538-4357/ab042c](https://doi.org/10.3847/1538-4357/ab042c)
- Jayasinghe, T., Kochanek, C. S., Stanek, K. Z., et al. 2018, *MNRAS*, 477, 3145, doi: [10.1093/mnras/sty838](https://doi.org/10.1093/mnras/sty838)
- Jiang, N., Dou, L., Wang, T., et al. 2016, *ApJL*, 828, L14, doi: [10.3847/2041-8205/828/1/L14](https://doi.org/10.3847/2041-8205/828/1/L14)
- Jiang, N., Wang, T., Hu, X., et al. 2021, *ApJ*, 911, 31, doi: [10.3847/1538-4357/abe772](https://doi.org/10.3847/1538-4357/abe772)
- Kochanek, C. S., Shappee, B. J., Stanek, K. Z., et al. 2017, *PASP*, 129, 104502, doi: [10.1088/1538-3873/aa80d9](https://doi.org/10.1088/1538-3873/aa80d9)
- König, O., Saxton, R. D., Kretschmar, P., et al. 2022, *Astronomy and Computing*, 38, 100529, doi: [10.1016/j.ascom.2021.100529](https://doi.org/10.1016/j.ascom.2021.100529)
- Kormendy, J., & Ho, L. C. 2013, *ARA&A*, 51, 511, doi: [10.1146/annurev-astro-082708-101811](https://doi.org/10.1146/annurev-astro-082708-101811)
- Kraft, R. P., Burrows, D. N., & Nousek, J. A. 1991, *ApJ*, 374, 344, doi: [10.1086/170124](https://doi.org/10.1086/170124)
- Lacy, M., Baum, S. A., Chandler, C. J., et al. 2020, *PASP*, 132, 035001, doi: [10.1088/1538-3873/ab63eb](https://doi.org/10.1088/1538-3873/ab63eb)
- Law-Smith, J., MacLeod, M., Guillochon, J., Macias, P., & Ramirez-Ruiz, E. 2017, *ApJ*, 841, 132, doi: [10.3847/1538-4357/aa6ffb](https://doi.org/10.3847/1538-4357/aa6ffb)
- Leloudas, G., Dai, L., Arcavi, I., et al. 2019, *ApJ*, 887, 218, doi: [10.3847/1538-4357/ab5792](https://doi.org/10.3847/1538-4357/ab5792)
- Lin, Z., Jiang, N., & Kong, X. 2022, *MNRAS*, 513, 2422, doi: [10.1093/mnras/stac946](https://doi.org/10.1093/mnras/stac946)
- Liu, F. K., Cao, C. Y., Abramowicz, M. A., et al. 2021, *ApJ*, 908, 179, doi: [10.3847/1538-4357/abd2b6](https://doi.org/10.3847/1538-4357/abd2b6)
- Liu, Z., Malyali, A., Krumpke, M., et al. 2023, *A&A*, 669, A75, doi: [10.1051/0004-6361/202244805](https://doi.org/10.1051/0004-6361/202244805)
- Liu, Z., Ryu, T., Goodwin, A. J., et al. 2024, arXiv e-prints, arXiv:2401.14091, doi: [10.48550/arXiv.2401.14091](https://doi.org/10.48550/arXiv.2401.14091)
- Lu, W., & Bonnerot, C. 2020, *MNRAS*, 492, 686, doi: [10.1093/mnras/stz3405](https://doi.org/10.1093/mnras/stz3405)

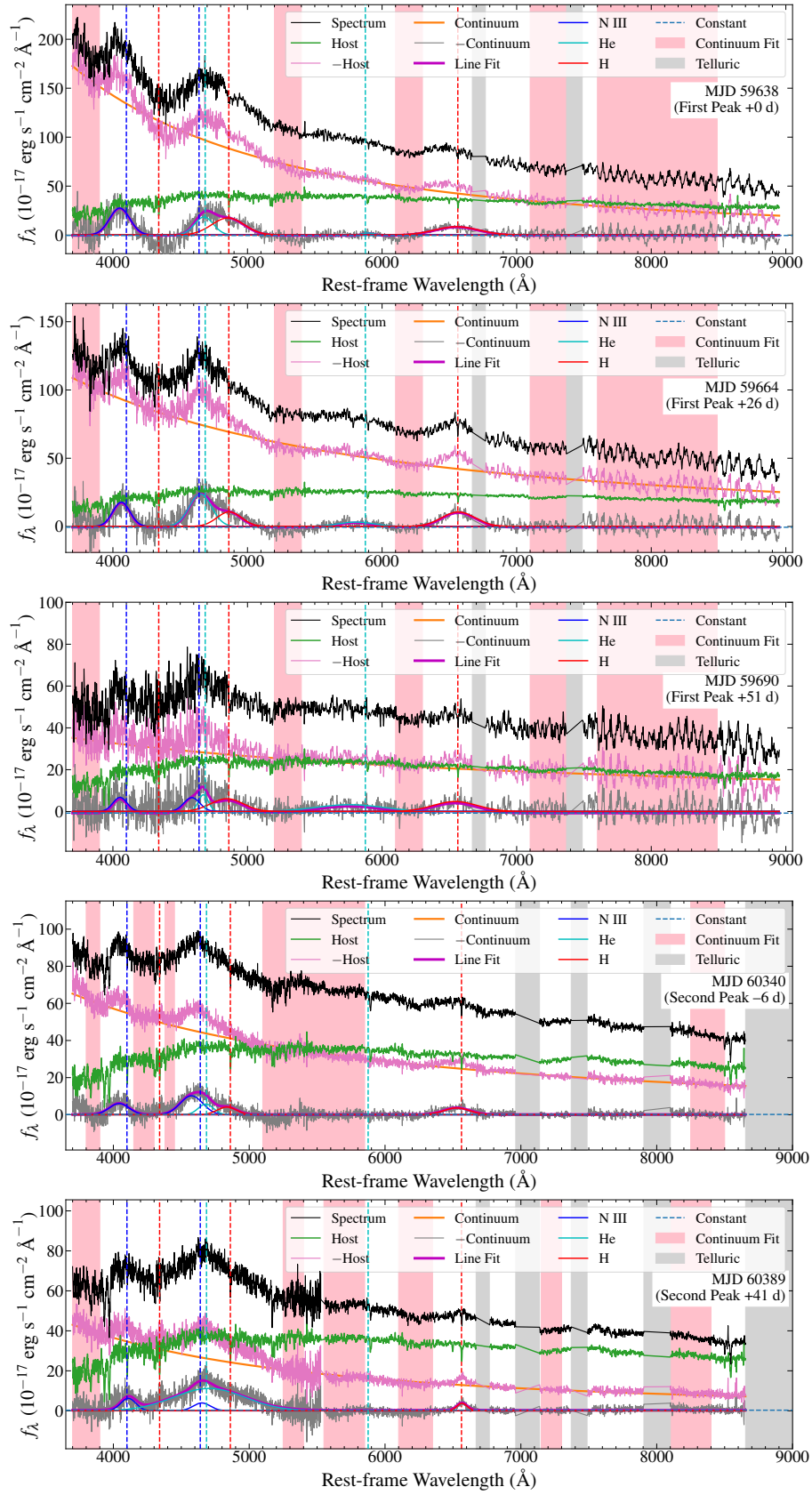


Figure A1. The fitting plots for optical spectra of AT 2022dbl.

- Mainzer, A., Bauer, J., Grav, T., et al. 2011, *ApJ*, 731, 53, doi: [10.1088/0004-637X/731/1/53](https://doi.org/10.1088/0004-637X/731/1/53)
- Mainzer, A., Bauer, J., Cutri, R. M., et al. 2014, *ApJ*, 792, 30, doi: [10.1088/0004-637X/792/1/30](https://doi.org/10.1088/0004-637X/792/1/30)
- Malyali, A., Liu, Z., Rau, A., et al. 2023, *MNRAS*, 520, 3549, doi: [10.1093/mnras/stad022](https://doi.org/10.1093/mnras/stad022)
- Mandel, I., & Levin, Y. 2015, *ApJL*, 805, L4, doi: [10.1088/2041-8205/805/1/L4](https://doi.org/10.1088/2041-8205/805/1/L4)
- Masci, F. J., Laher, R. R., Rusholme, B., et al. 2019, *PASP*, 131, 018003, doi: [10.1088/1538-3873/aae8ac](https://doi.org/10.1088/1538-3873/aae8ac)
- Metzger, B. D., & Stone, N. C. 2016, *MNRAS*, 461, 948, doi: [10.1093/mnras/stw1394](https://doi.org/10.1093/mnras/stw1394)
- Nicholl, M. 2018, *Research Notes of the American Astronomical Society*, 2, 230, doi: [10.3847/2515-5172/aaf799](https://doi.org/10.3847/2515-5172/aaf799)
- Oke, J. B. 1974, *ApJS*, 27, 21, doi: [10.1086/190287](https://doi.org/10.1086/190287)
- Oke, J. B., & Gunn, J. E. 1982, *PASP*, 94, 586, doi: [10.1086/131027](https://doi.org/10.1086/131027)
- Osterbrock, D. E., & Ferland, G. J. 2006, *Astrophysics of gaseous nebulae and active galactic nuclei*
- Payne, A. V., Shappee, B. J., Hinkle, J. T., et al. 2021, *ApJ*, 910, 125, doi: [10.3847/1538-4357/abe38d](https://doi.org/10.3847/1538-4357/abe38d)
- , 2022, *ApJ*, 926, 142, doi: [10.3847/1538-4357/ac480c](https://doi.org/10.3847/1538-4357/ac480c)
- Payne, A. V., Auchettl, K., Shappee, B. J., et al. 2023, *ApJ*, 951, 134, doi: [10.3847/1538-4357/acd455](https://doi.org/10.3847/1538-4357/acd455)
- Pfister, H., Volonteri, M., Dai, J. L., & Colpi, M. 2020, *MNRAS*, 497, 2276, doi: [10.1093/mnras/staa1962](https://doi.org/10.1093/mnras/staa1962)
- Piran, T., Svirski, G., Krolik, J., Cheng, R. M., & Shiokawa, H. 2015, *ApJ*, 806, 164, doi: [10.1088/0004-637X/806/2/164](https://doi.org/10.1088/0004-637X/806/2/164)
- Planck Collaboration, Aghanim, N., Ashdown, M., et al. 2016, *A&A*, 596, A109, doi: [10.1051/0004-6361/201629022](https://doi.org/10.1051/0004-6361/201629022)
- Prabhu, T. P. 2014, *Proceedings of the Indian National Science Academy Part A*, 80, 887, doi: [10.16943/ptinsa/2014/v80i4/55174](https://doi.org/10.16943/ptinsa/2014/v80i4/55174)
- Prochaska, J., Hennawi, J., Westfall, K., et al. 2020, *The Journal of Open Source Software*, 5, 2308, doi: [10.21105/joss.02308](https://doi.org/10.21105/joss.02308)
- Rees, M. J. 1988, *Nature*, 333, 523, doi: [10.1038/333523a0](https://doi.org/10.1038/333523a0)
- Reines, A. E., & Volonteri, M. 2015, *ApJ*, 813, 82, doi: [10.1088/0004-637X/813/2/82](https://doi.org/10.1088/0004-637X/813/2/82)
- Roming, P. W. A., Kennedy, T. E., Mason, K. O., et al. 2005, *SSRv*, 120, 95, doi: [10.1007/s11214-005-5095-4](https://doi.org/10.1007/s11214-005-5095-4)
- Sfaradi, I., Horesh, A., & Fender, R. 2022, *Transient Name Server AstroNote*, 57, 1
- Shappee, B. J., Prieto, J. L., Grupe, D., et al. 2014, *ApJ*, 788, 48, doi: [10.1088/0004-637X/788/1/48](https://doi.org/10.1088/0004-637X/788/1/48)
- Shingles, L., Smith, K. W., Young, D. R., et al. 2021, *Transient Name Server AstroNote*, 7, 1
- Singh, A. 2021, *RedPipe: Reduction Pipeline*. <http://ascl.net/2106.024>
- Smith, K. W., Smartt, S. J., Young, D. R., et al. 2020, *PASP*, 132, 085002, doi: [10.1088/1538-3873/ab936e](https://doi.org/10.1088/1538-3873/ab936e)
- Somalwar, J. J., Ravi, V., & Lu, W. 2023a, arXiv e-prints, arXiv:2310.03795, doi: [10.48550/arXiv.2310.03795](https://doi.org/10.48550/arXiv.2310.03795)
- Somalwar, J. J., Ravi, V., Yao, Y., et al. 2023b, arXiv e-prints, arXiv:2310.03782, doi: [10.48550/arXiv.2310.03782](https://doi.org/10.48550/arXiv.2310.03782)
- Stone, N. C., & Metzger, B. D. 2016, *MNRAS*, 455, 859, doi: [10.1093/mnras/stv2281](https://doi.org/10.1093/mnras/stv2281)
- Stone, N. C., Vasiliev, E., Kesden, M., et al. 2020, *SSRv*, 216, 35, doi: [10.1007/s11214-020-00651-4](https://doi.org/10.1007/s11214-020-00651-4)
- Thomsen, L. L., Kwan, T. M., Dai, L., et al. 2022, *ApJL*, 937, L28, doi: [10.3847/2041-8213/ac911f](https://doi.org/10.3847/2041-8213/ac911f)
- Tonry, J. L., Denneau, L., Heinze, A. N., et al. 2018, *PASP*, 130, 064505, doi: [10.1088/1538-3873/aabadf](https://doi.org/10.1088/1538-3873/aabadf)
- van Velzen, S., Holoiën, T. W. S., Onori, F., Hung, T., & Arcavi, I. 2020, *SSRv*, 216, 124, doi: [10.1007/s11214-020-00753-z](https://doi.org/10.1007/s11214-020-00753-z)
- van Velzen, S., Mendez, A. J., Krolik, J. H., & Gorjian, V. 2016, *ApJ*, 829, 19, doi: [10.3847/0004-637X/829/1/19](https://doi.org/10.3847/0004-637X/829/1/19)
- van Velzen, S., Gezari, S., Hammerstein, E., et al. 2021, *ApJ*, 908, 4, doi: [10.3847/1538-4357/abc258](https://doi.org/10.3847/1538-4357/abc258)
- Wang, J., & Merritt, D. 2004, *ApJ*, 600, 149, doi: [10.1086/379767](https://doi.org/10.1086/379767)
- Wang, M., Ma, Y., Wu, Q., & Jiang, N. 2024, *ApJ*, 960, 69, doi: [10.3847/1538-4357/ad0bfb](https://doi.org/10.3847/1538-4357/ad0bfb)
- Wang, T., Liu, G., Cai, Z., et al. 2023, *Science China Physics, Mechanics, and Astronomy*, 66, 109512, doi: [10.1007/s11433-023-2197-5](https://doi.org/10.1007/s11433-023-2197-5)
- Wevers, T., Pasham, D. R., van Velzen, S., et al. 2019, *MNRAS*, 488, 4816, doi: [10.1093/mnras/stz1976](https://doi.org/10.1093/mnras/stz1976)
- Wevers, T., Coughlin, E. R., Pasham, D. R., et al. 2023, *ApJL*, 942, L33, doi: [10.3847/2041-8213/ac9f36](https://doi.org/10.3847/2041-8213/ac9f36)
- Wright, E. L., Eisenhardt, P. R. M., Mainzer, A. K., et al. 2010, *AJ*, 140, 1868, doi: [10.1088/0004-6256/140/6/1868](https://doi.org/10.1088/0004-6256/140/6/1868)
- Wu, X.-J., & Yuan, Y.-F. 2018, *MNRAS*, 479, 1569, doi: [10.1093/mnras/sty1423](https://doi.org/10.1093/mnras/sty1423)
- Yao, Y., Ravi, V., Gezari, S., et al. 2023, *ApJL*, 955, L6, doi: [10.3847/2041-8213/acf216](https://doi.org/10.3847/2041-8213/acf216)
- Zhong, S., Li, S., Berczik, P., & Spurzem, R. 2022, *ApJ*, 933, 96, doi: [10.3847/1538-4357/ac71ad](https://doi.org/10.3847/1538-4357/ac71ad)
- Zhu, J., Jiang, N., Wang, T., et al. 2023, *ApJL*, 952, L35, doi: [10.3847/2041-8213/ace625](https://doi.org/10.3847/2041-8213/ace625)